1. Summary

IL9906628

Passive Cooling Systems in Power Reactors

J. Aharon, R. Harari, M. Haim, Y. Weiss, Y. Barnea, M. Katz and M. Szanto

This paper reviews several R&D activities associated with the subject of passive cooling systems, conducted by the N.R.C.Negev thermohydraulic group. A short introduction considering different types of thermosyphons and their applications is followed by a detailed description of the experimental work, its results and conclusions. An ongoing research project is focused on the evaluation of the external dry air passive containment cooling system (PCCS) in the AP-600 (Westinghouse advanced pressurized water reactor). In this context some preliminary theoretical results and planned experimental research are for the fature described.

2. Introduction

The basic design requirement of novel cooling systems in nuclear applications inherent safety. Self-operating cooling systems are needed during all stages of the fuel life cycle. These Passive Cooling Systems (PCS) are used in the nuclear industry in order to act upon the overheated reactor facilities in the wake of any possible event of emergency scenarios, as well as to cool spent fuel in various storage configurations.

The main characteristic of the PCS is that they do not rely on blowers or pumps for fluid circulation. Rather, the flow is circulated by the buoyancy forces resulting from density gradients due to heat transfer processes from fission products. The circular flow patterns and the resulting heat transfer mechanisms, are termed Induced Mixed Convection

(IMC)[1]. In this phenomenon, defined within a confined space, a buoyancy driven flow adjacent to the surface, caused by the heat transfer, induces a secondary flow in the fluid core. The secondary flow can be of the aiding or "opposed" type, depending on the external flow direction.

These thermally derived systems are often called thermosyphons and are used in many engineering applications with various configurations. There are two major types of thermosyphons: one in which the working fluid is simply contained in a closed or partially closed container, forming a cooling cycle along its boundaries (Fig. 1); and another in which the flow is thermally induced through channels, forming an open or closed loop (Fig. 2). In systems classified as the first type, the heat and momentum transfer process is driven by utilizing buoyancy forces on a fluid contained in a vessel. Therefore, a net heat transfer, at suitable points, is required for continuous operation and mechanical inputs are excluded. Figure 1 shows two types of thermosyphons which were investigated.
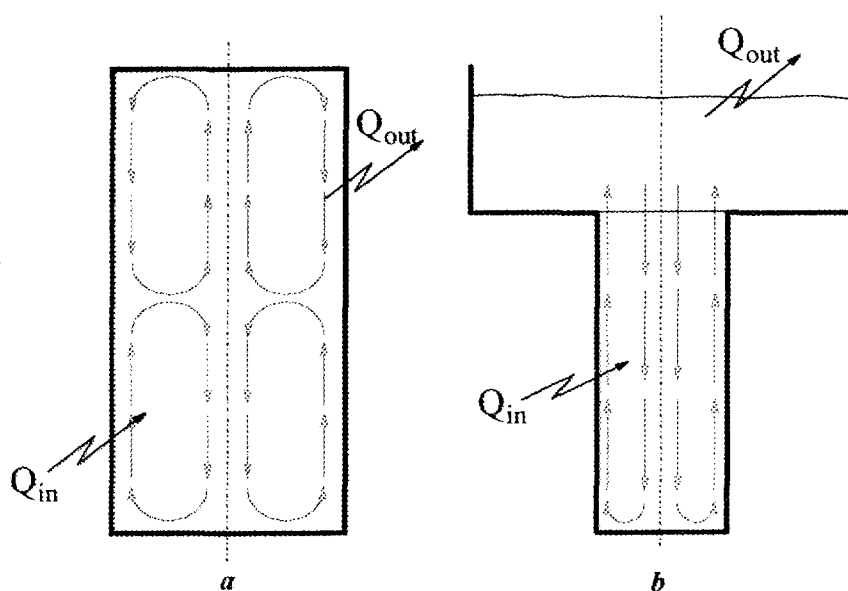

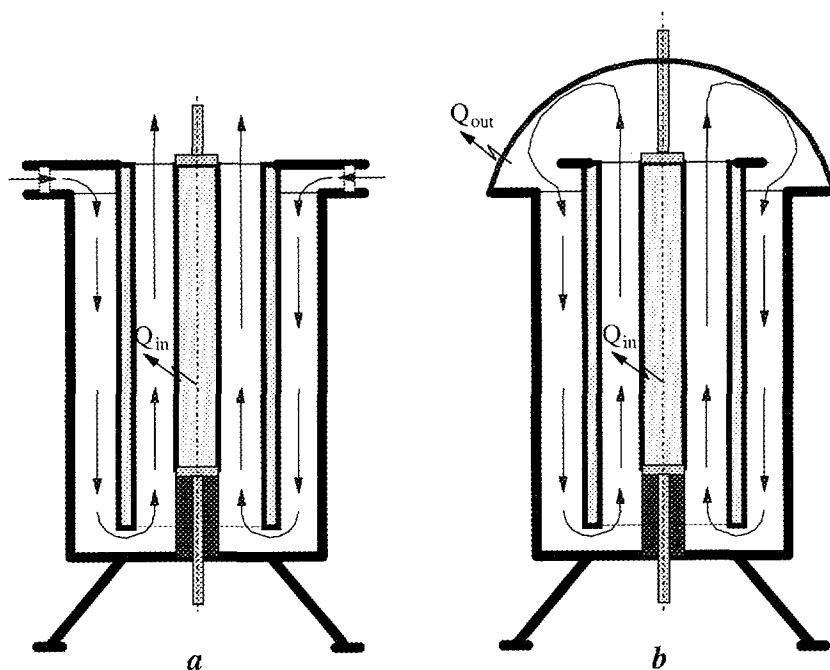*Fig.1: The closed (a) and an open (b) thermosyphon.*

*Fig.2: An open (a) and a closed
(b) loop thermosyphon*

The thermosyphons are purely free convection devices, being either open or closed. The open system is basically more efficient, since it is capable of removing higher heat transfer rates. For example, in the case of an emergency loss of cooling event in a nuclear reactor, it is necessary to remove large amounts of heat as quickly as possible. Thus, cooling the reactor by using an open thermosyphon connected to a common industrial water supply located on the building's roof seems to be quite feasible. The water supply would form a natural reservoir for an open thermosyphon and would allow the discharge of a large amount of energy in it.

Similarly, passive heat removal from gas-cooled nuclear reactors (HTGR and HTR), during a postulated Loss of Cooling Accident, requires various engineering solutions such as a Hot Gas Duct (HGD). The HGD is a preheated

cylindrical duct, located higher than the nuclear reactor core to enable the removal of the decay heat by a process of natural thermosyphon cycle. During normal operating conditions the lower plenum is heated to compensate for external heat losses and to maintain along the HGD, a constant temperature necessary to direct the flow in the passive cooling cycle. A buoyancy-driven downward flow adjacent to the inner surface, caused by the external heat transfer to the surroundings, may induce an opposed upper flow in the duct's core. That possible flow generates an overall Opposed Induced Mixed Convection (OIMC) effect and, consequently, the undesired axial temperature gradient.

The open thermosyphon is another system, in which a similar heat transfer process takes place. There an OIMC flow field is developed by heating circumferencially a vertical tube closed at its bottom and open at the top to a large reservoir.

Understanding the interaction between the flow adjacent to the tube's wall and the opposed induced flow at the core, was a challenging subject for many researchers. Referring to a similar heat transfer process, Lighthill[2] solved analytically the problem of cooling turbine blades, as convective flow in narrow vertical tubes, with constant outside wall temperature. The author employed an integral momentum boundary layer analysis to describe various laminar and turbulent flow regimes. Evans et al.[3] reported a similar analytical and experimental study, of transient natural convection in a vertical cylinder. An analytical model was developed by dividing the system into three regions: a thin boundary layer rising along the heated walls;

a mixing region at the top where the boundary layer discharges and mixes with the fluid at the upper core; and a main core region which slowly falls as plug flow. Japikse and Winter[4] reported a theoretical and experimental study of the boundary layer heat transfer in an open thermosyphon, recommending some practical correlations to determine the laminar and turbulent flow regimes as well as the transition zone. Ostrach[5] reviewed the natural convection phenomenon in enclosures, pointing out that the interactions between the boundary layer and the core remain an unsolved problem, inherent to all confined convection configurations. Recently, Weiss et al.[6] analyzed the OIMC phenomenon by a theoretical model, assuming boundary layer type of flow in the turbulent regime, and found that such a model is defined only over a certain domain. Additionally, further downstream, different heat transfer regimes are anticipated. In order to characterize all possible existing flow regimes, an advanced numerical simulation in the turbulent flow regime was carried out[1], providing a good fit to the experimental results [1,7,8].

Systems related to the second type of thermosyphon (Fig.2), use natural convection to generate flow within the system channels, forming an overall Aiding Induced Mixed Convection (AIMC) or OIMC effect. For example, in the open loop thermosyphon (Fig. 2a), the inner channel is clearly dominated by natural convection phenomena. The flow within the channels is a combination of forced and free convection. The forced convection flow component is the result of the fluid being drawn through the external channel by the buoyancy forces in the inner channel. Based on this

phenomenon, the Westinghouse AP-600 reactor design uses such a type of passive containment cooling system. The air flow path designed between the steel reactor containment hot shell and the concrete shield building, creates an open loop thermosyphon. External cold air is introduced through specially designed shutters located at the upper level of the concrete shield building, while cooling the hot steel containment generates an induced upward air flow.

Various studies of different types of natural circulation loops were reviewed by Mertol and Greif [9]. For this type of system, work related to natural convection on vertical plates, vertical cylinders, between vertical parallel plates and in vertical tubes was considered. These configurations represent the basic mechanisms associated with natural or induced mixed convection in the system.

Understanding the influence of boundary conditions on natural convection along the containing walls is very important. In a large number of these applications the surface heating conditions are non-uniform i.e., the natural convection on one side of the wall is coupled with another heat transfer mechanism on the other side. Aharon and co-workers [10,11] measured the heat transfer coefficient for free convection on a vertical plate with general boundary conditions (neither constant temperature nor constant heat flux). In these experiments coupling between free convection and other heat transfer processes, taking place on the other side of the plate, was investigated.

Referring to natural circulating loops, the commonly used basic assumption is that the induced flow is fully

developed. However, it must be recognized that full development cannot be expected at all elevations in the channel but only above a certain distance from the channel entrance. Considering the developing flow region higher heat transfer coefficient are obtained.

Bodoia and Osterle[12], Bar-Cohen and Rohsenow[13], Burch et al.[14] and Webb and Hill[15] analyzed the development of the induced flow between vertical parallel plates. Davis and Perona[16] analyzed numerically the development of the induced flow in a heated vertical open tube. From the velocity and temperature profiles obtained for various stages of the flow development, a graphical correlation between volumetric flowrate and heat transfer rates was found.

Clarksean[17] analyzed experimentally the characteristics of a thermosyphon designed to cool cylindrical spent fuel heat sources passively. The analysis is based on recognizing the physics of the flow within different regions of the thermosyphon in order to develop empirical heat transfer correlations. Considering the external dry air passive containment cooling of the AP-600 reactor, Barnea et. al[18] and Harari et. al.[19] developed a theoretical model to predict pressure drop, mass flowrate, hot surface temperature and heat transfer coefficient behavior in an open loop thermosyphon configuration. This theoretical model served to optimize the design of an experimental system in order to verify the calculated parameters.

Buoyancy induced flows are complex because of the essential coupling between the flow and energy transport phenomena. These flow fields can be classified as either external (free convection) or internal (natural convection). The PCS are basically natural convection problems, that is classed as an internal problem. Internal problems are considerably more complex than external ones, because the region external to the boundary layer is affected by the boundary layer itself. The interaction between the boundary layer and the external flow field constitutes a central problem in determining the heat transfer coefficient. Furthermore, the flow pattern and the resulting heat transfer mechanism cannot be predicted a priori from the given boundary conditions and geometry.

Experimental measurements in this complex flow and heat transfer field are very difficult. Using conventional measuring probes may introduce disturbances, which can cause cardinal changes in the entire flow field. most complicated parameters to measure are the velocity profiles, which are an essential tool for determining different types of flow regimes. Therefore, the best way to overcome the mentioned difficulties is to combine temperature profile measurements, flow visualization and advanced numerical simulation results.

Some of the experimental systems that were built to evaluate the feasibility of these passive cooling systems are presented herein. along with, describing the experimental apparatus buildup, highlighting some measurement difficulties, and reporting the typical results. Some of these experimental systems are still part of an ongoing research

program carried out in the Thermohydraulics Laboratory at NRC-Negev.

Considering a vertical flat plate that on one side transfers heat by natural convection to a fluid at temperature T_∞ at a general boundary condition, namely, the other side of the plate is exposed to an environment of a constant temperature, T_a, with which heat is exchanged with an effective heat transfer coefficient (h_{eq}). In engineering solutions for heat transfer problems, the effective heat transfer coefficient could be the result of a forced convection or one-dimensional conduction in the wall.

The apparatus used in the experiments is shown schematically in Figure 3. The experimental plate consists of three layers: the exposed stainless steel plate, the aluminum isothermal plate and an insulation layer between the two plates. The exposed plate, which is the heat transferring surface, is 600 mm wide x1020 mm high and x0.5 mm thick; it dissipates the heat to the surroundings. The isothermal plate is 600 mm wide x1020 mm high x 6 mm thick. The high thermal conductivity of the aluminum and the fact that the aluminum plate is 6 mm thick, make it possible to maintain the plate at uniform temperature. Eight pairs of heating strips are bonded to the back side of the isothermal plate. Each pair had a temperature controller to keep all the heating zones at a uniform temperature.

3. Experimental systems and results

3.1 The effect of boundary conditions on free convection

Fig. 3: Schematic diagram of the experimental apparatus: (1) Perspex test chamber, (2) stainless steel plate, (3) insulation layer - h_{eq}, (4) isothermal plate, (5) heaters, (6) backup rock wool insulation, (7) temperature controller, (8) temperature measuring instrument, (9) hot wire anemometer.
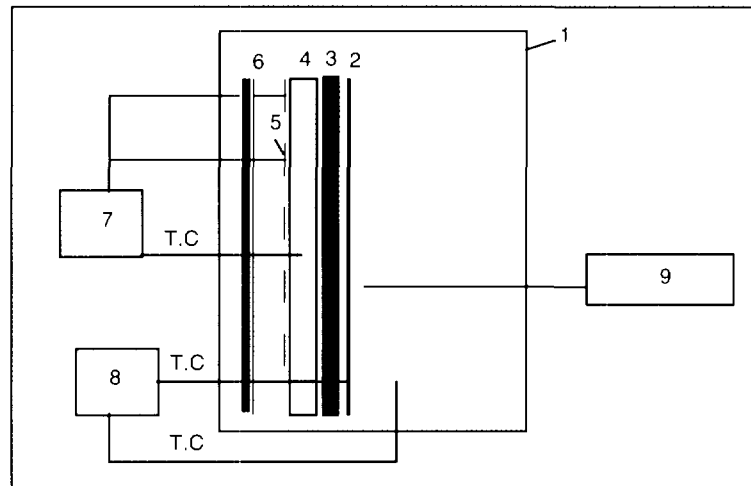
The constant temperature of the aluminum plate represents the hot temperature- T_a. A couple of ceramic paper layers, each 3 mm thick with a thermal conductivity of ~0.08 W/m-°C, was inserted between the aluminum and the stainless steel plates. These insulation layers have an effective heat transfer coefficient, h_{eq}, the value of which can be altered by changing the number of the insulating layers.

In order to measure the surface temperature of the stainless steel plate (the exposed surface), 20 chromel alumel thermocouples of ~1 mm diam. were brazed on the surface. The junctions of these thermocouples were placed in the vertical direction along the center line of the plate. In order to measure and control the temperature of the aluminum plate, eight thermocouples were connected to the plate covering the entire controlled heating zone. To reduce heat loss from the rear of the plate, two 50mm layers of rock wool insulation were installed on the back side of the heaters and the isothermal plate. Temperature stratification in the test chamber was measured by the use of K- type

thermocouples,(see Fig. 3).

Experiments were carried out in the closed Perspex chamber to avoid any air currents; the chamber and the measuring instruments are shown in Figure 4.
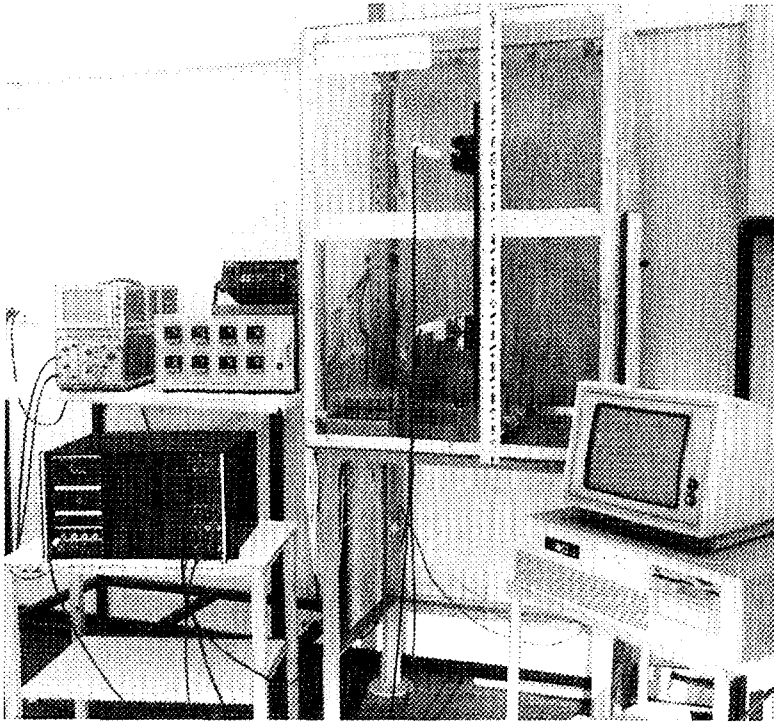

Fig. 4: The test chamber and measuring instruments

The figure shows a plot of the experimental data for the three values of, h_{eq} in which the results are plotted as log Nu vs. log Ra^*, where:

$$Ra^* = \frac{h_{eq}}{h(x) + h_{eq}} \cdot \frac{g\beta(T_a - T_\infty)x^3}{v^2} \cdot Pr \qquad (1)$$

Figure 5 covers a range of local Rayleigh numbers between 1.3×10^5 and 2.46×10^8 and the results for various - h_{eq} values are denoted by different symbols.

Fig. 5: Free-convection heat-transfer correlation for heat transfer from a heated vertical plate.
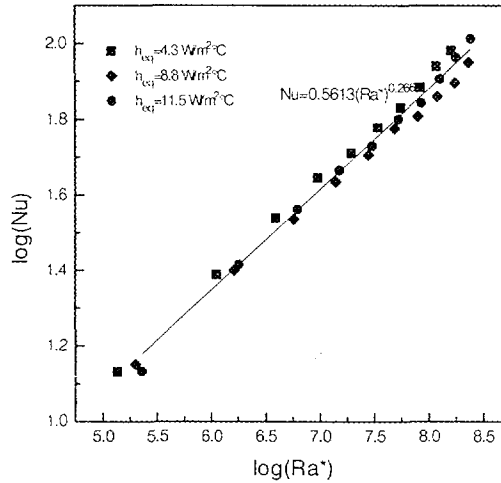
The linear least squares fit of log (Nu) or a function of (Ra*) yields the following correlation

$$Nu = 0.5613 \cdot \left(Ra *\right)^{0.266} \qquad (2)$$

for which the deviation of a single experimental value from the fitted value did not exceed 12%.

3.2 Flow and heat transfer characteristics of the OIMC phenomenon

The research was focused on the OIMC phenomenon, i.e. the flow field structure in a vertical cylinder, closed at the bottom and open at the top, and being heated circumferentially. To achieve a better understanding of the flow field and the related heat-transfer process, two different experimental systems were built. The first was a flow visualization system, with water as the working fluid, whereas the second system enabled quantitative measurements of the temperature field in air. Experiments were performed in the turbulent flow regime. In order to learn about all possible flow regimes, the visualization tests were conducted at three different length-to-diameter ratios

(L/D=1, 5, 10). Quantitative measurements of the cylindrical wall temperature, as well as of the radial and axial temperature profiles in the flow field, were taken in the air system.

The apparatus used, shown schematically in Figure 6, consists of a heated vertical cylinder closed at the bottom and open at the top to the surroundings. The test section was a stainless-steel cylinder, 25cm I.D, x 125cm high x 4mm thick. Along the cylinder's wall, in the vertical direction, 16 2mm-diam. holes were drilled at intervals of 10 and 5cm in the lower and upper halves, respectively;. one type-K thermocouple was soldered at each of these holes. An additional 16 type-K thermocouples were inserted at the same intervals along the centerline. They were attached to a vertically mounted thin rod, 5mm in diameter. Radial temperature distribution was obtained at three different vertical levels by additional moveable thermocouples, attached to a mechanical traversing system. The thermocouples were guided radially, through the wall of the cylinder, by special tubes welded opposite each soldered thermocouple. Temperatures were measured simultaneously at three different levels.
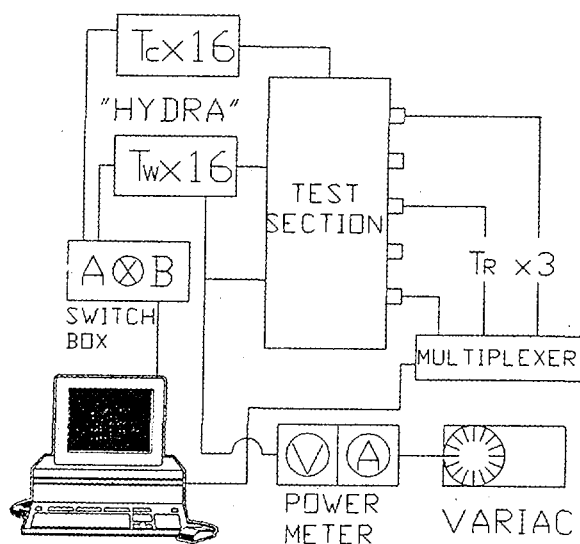

Fig. 6: The experimental apparatus for quantitative measurements in air

Six identical electrical heating blankets were used to create constant heat flux at the wall. They were connected through a power measuring device to a Variac transformer. A 5cm thick blanket of glass wool was used to insulate the test section in the radial direction. The cylindrical test section was based on a 10cm thick plate of wood, sealing the bottom and serving as a thermal insulator.

The wall and centerline thermocouples were connected to two multichannel measuring devices (Hydra, Fluke) and, through a switch box, to the computer. The three radial probes were connected through a multiplexed box to a DAQ card (both National Instrument products) on the same computer. The data were collected simultaneously from the probes by a DAQ software Lab VIEW^{TM}. The software enabled us to control the scan rate as well as to average values measured at each point. Calibration experiments to estimate the system's heat loss had been carried out previously.

The net input heat flux (q'') was obtained by subtracting the external heat loss from the gross heat electrical input. The initial procedure for each test involved heating the cylinder until steady-state conditions were established.

Three radial temperature probes were moved simultaneously in the radial direction, starting from the wall and going backward toward the centerline. During the radial temperature measurements, wall and centerline temperature profiles were sampled simultaneously by the computer at fixed time intervals.

In order to study the possible flow regimes, a visualization apparatus (Fig. 7) was built. It consists of a thin glass tube, 40mm I.D. sealed by a rubber plug at the bottom. The open end was connected to the base of a cold reservoir fabricated from Perspex. The cold reservoir, with its glass tube extension, was mounted on top of a hot water reservoir. Steady state was achieved in the hot water reservoir by circulating the water through an electrically heated bath. Three different glass tubes were used to form three length to diameter ratios (L/D=1, 5, 10). To trace the developed patterns of flow, $KMnO_4$ crystals were dropped to the bottom of the tube. The experiments were carried out while heat was transferred between the two reservoirs, through the thin glass tube.
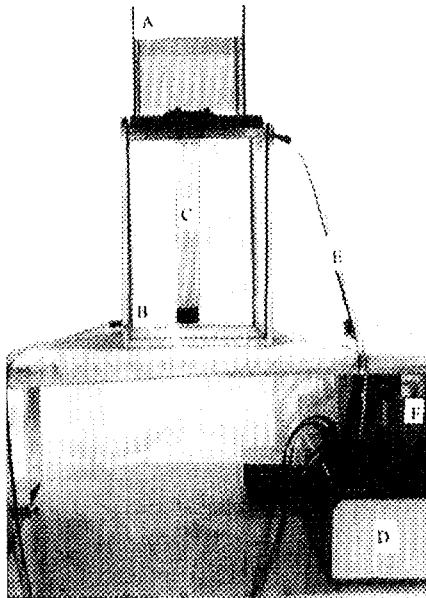
Fig. 7: The flow visualization apparatus

In the cold air system the measured temperature profiles were normalized as:

$$T^* = \frac{T - T_0}{q''d / k} \qquad (3)$$

where T_0 is the temperature measured at the tube entry region and $q''d/k$ is a characteristic temperature difference for the constant heat flux case. This characteristic temperature difference is determined from (a) the net heat flux transferred by convection (q''), (b) the tube diameter, and (c) the air thermal conductivity taken at the entry condition. Two typical radial temperature profiles at two levels along the tube are presented in Figures 8 and 9, respectively, for $Ra_d^*=5\times10^8$. From these temperature profiles it is understood that a radial temperature profile typical to a boundary layer exists at lower levels of the tube, whereas near the entry levels, radial gradients were observed up to the centerline. Wall temperature profiles for three different heat fluxes are presented in Figure 10. Referring to the measured wall temperature profile, three different regimes of heat transfer are observed. The wall temperature increases from the bottom of the tube, until a maximum is reached at approximately $x/d=1$ (zone 1). At this zone a better heat transfer mechanism takes place, and the temperature decreases in a moderate slope (zone 2). The third regime is determined between $x/d\cong3$ and $x/d=5$ and is characterized by a sharper decrease in wall temperature. Based on numerical simulation results, visualization and the measured temperature profiles, it was found that the OIMC can be characterized by three main regimes.
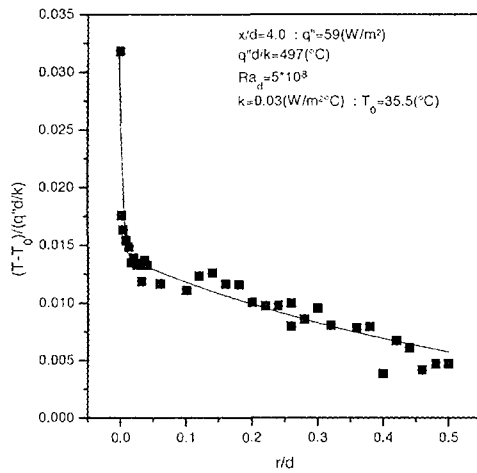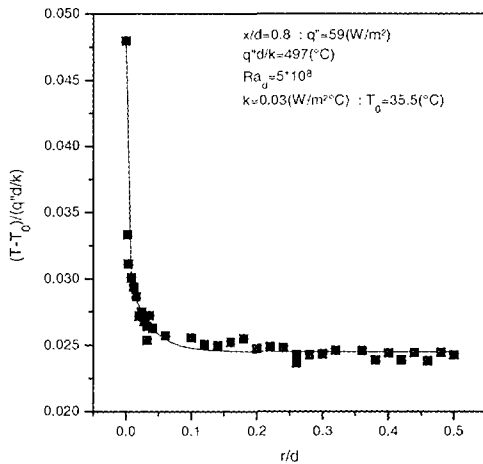
Fig. 8: Radial temperature profile at $x/d=4.0$

Fig. 9: Radial temperature profile at $x/d=0.8$

The first regime, at the bottom, constitutes a boundary layer type of flow adjacent to the heated wall. The second regime, above the first, behaves like a direct contact counter flow heat exchanger. This regime is characterized by a similar velocity and temperature profiles at each section of the cylinder. The third is a mixing regime at the entry region of the cylinder.

Under certain conditions the cold fluid from the reservoir did not penetrate into the cylinder's core. Actually,

an enhanced mixing heat transfer process takes place at the boundary between the cylinder and the reservoir, forming a "separation interface". The mixing causes the upcoming hot fluid to cool down, and return downward along the centerline of the cylinder, whereas the cold fluid in the reservoir is heated and rises upward at the reservoir centerline. Such behavior of the inlet flow field affects the efficiency of the cylinder as a passive cooling device. These findings are at odds with the basic assumption in the literature that the heated fluid adjacent to the wall is discharged from the open end into the cold reservoir, whereas a central core of cold fluid is continuously replacing the hot fluid, entering at the temperature of the reservoir.

Fig.10: Wall temperature profile at three different heat fluxes.
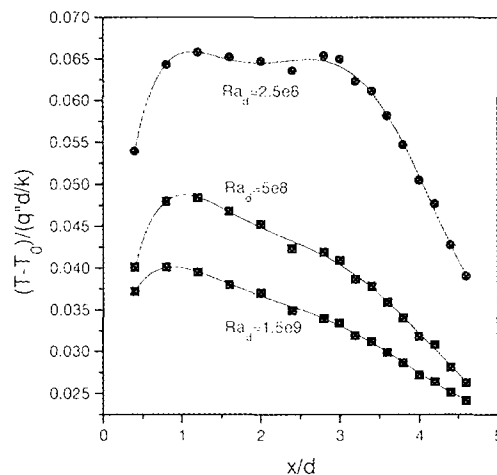
3.3 Flow and heat transfer characteristics of an open loop thermosyphon

An additional subject of interest and R&D activity is the gravity-driven passive safety systems type of the AP600 (Westinghouse advanced pressurized water reactor). An ongoing research is focused on the evaluation of the external dry air (PCCS). Primary theoretical models[18,19] were developed and used to calculate the mass flow rate of the

natural circulating air and the resultant heat transfer processes were proposed and evaluated. Based on these calculations, an experimental test was designed. The schematic description of the experimental apparatus assembled is presented in Fig. 11. The test section consists of an inner electrical heated metal pipe (Fig.12a) and an outer metal envelope (Figure 12b), simulating the containment and shield building respectively and creating a typical U-shape annular air flow path. The following parameters will be measured: (a) air inlet and outlet temperatures; (b) axial distribution of air mean velocity and temperature; (c) axial pressure drop; and (d) axial distribution of the temperature on the heated surface.

This planned research for the future is concerned with evaluating experimentally the calculated parametric trends and testing the fully developed flow assumption. The parameters trends are related to two items of interest: (i) Scaling-up the hydraulic diameter of both the hot and the cold channel by increasing the external diameter (D) by an order of magnitude (up to actual reactor containment size) and maintaining a constant hydraulic diameter along the flow path. (ii) Different ratios between the hot and cold channels' diameters ($D_{h1}/D_{h2} \neq 1$) and a possible optimal design. Referring to the hydraulic and thermal parameters (assuming fully developed flow in the channels), the mass flowrate and the overall pressure drop indicate maximum and minimum values, respectively, for $D_{h1}/D_{h2} \approx 0.5$ (Figs. 13,14), while a minimum value of the maximum temperature is obtained for $D_{h1}/D_{h2} \approx 2$ (Fig.15). The behavior of the heat transfer coefficient, taking into account

the possibility that the flow is in either the laminar or turbulent regime, is presented in Figure 16.
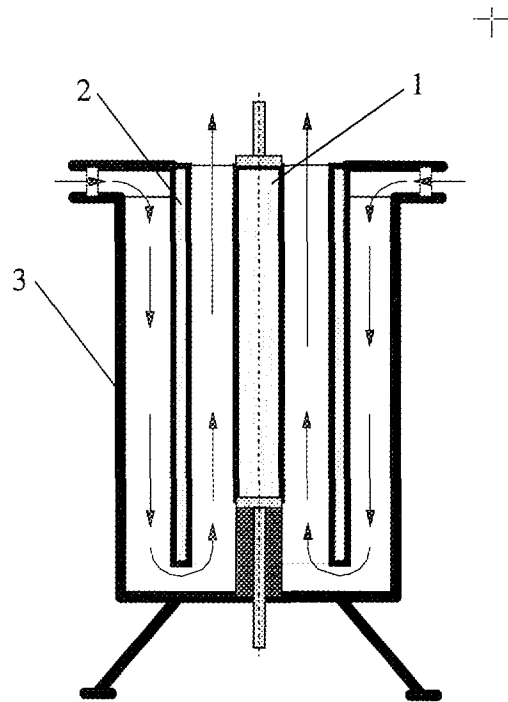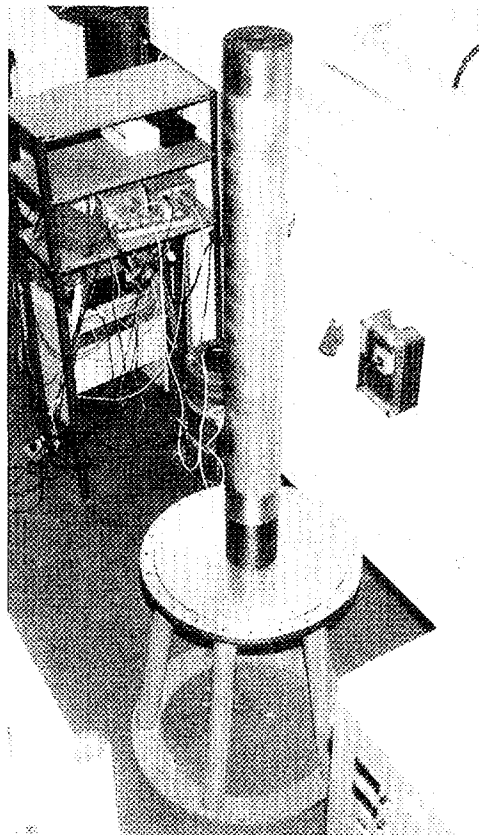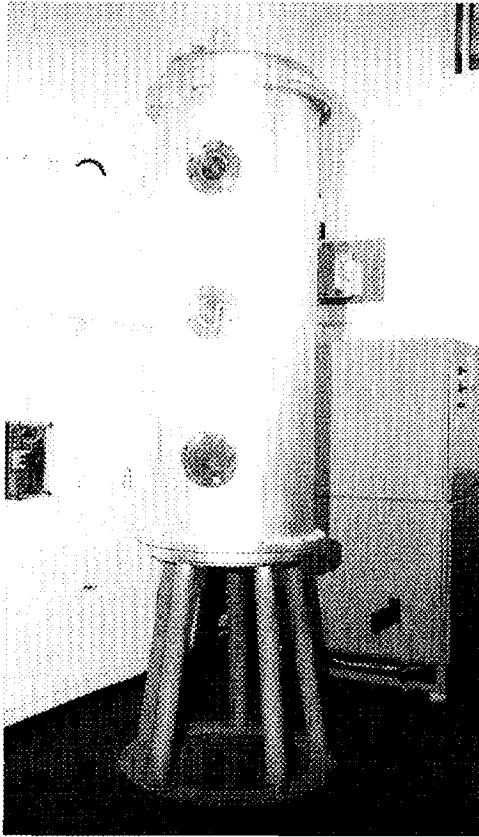
Fig. 11: Schematic description of the test section: (1) electrical heating pipe, (2) shield, (3) envelope

a

b

Fig.12 a) The electrical heating metal pipe; b) The outer metal envelope simulating the containment and shield building.
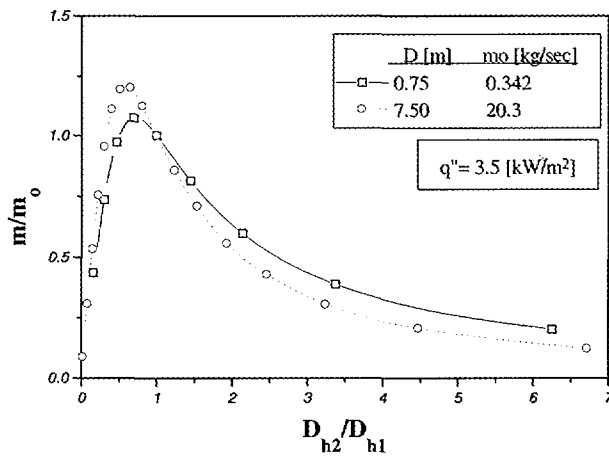

Fig. 13: Coolant mass flowrate vs. hydraulic diameter ratio.

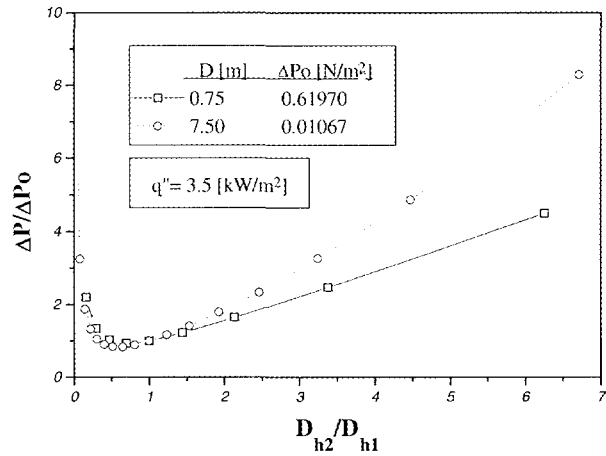*Fig. 14: Pressure drop vs. hydraulic diameter ratio.*

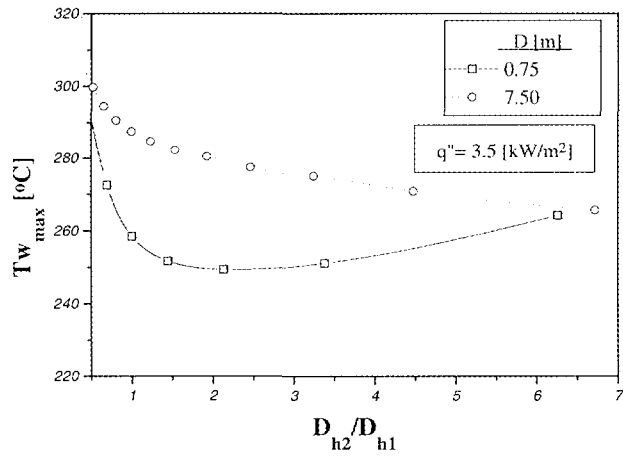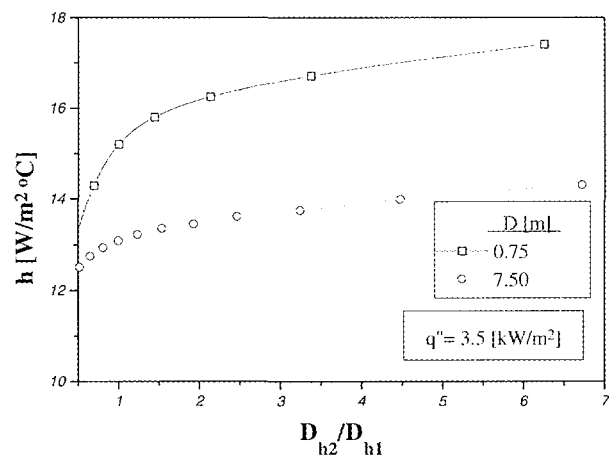*Fig. 15: Maximum surface temperature vs. hydraulic diameter ratio.*

Fig. 16: Convective heat transfer coefficient in the hot channel vs. hydraulic diameter ratio.

4. Nomenclature and subscripts

d - diameter
D - external diameter
g - gravity acceleration
h - convection heat transfer coefficient
L - length
m - mass
Nu_x - Nusselt number (hx/k)
P - pressure
Pr - Prandtl number (v/α)
k - thermal conductivity
q'' - heat flux
r - radial distance
x - axial distance
Ra_d^* - $g\beta q'' d^4/v\alpha\kappa$
T - temperature
α - thermal diffusivity
β - volumetric coefficient of thermal expansion.
v - kinematic viscosity
a - hot side
eq - equivalent
o - nominal (exp. test conditions)
h1 - hydraulic diameter of hot channel
h2 - hydraulic diameter of cold channel
w - wall condition
∞ - ambient, cold side

5. *References*

1. Y .Weiss, Analysis of Buoyancy-Induced Mixed Convection, Ph.D. Thesis, Ben-Gurion University of the Negev. Beer Sheva, Israel, October 1996.

2. M.J. Lighthill, Theoretical Considerations on Free Convection in Tubes, Q. J. Mech. Appl. Math. 4, 398-439 (1953).

3. L.B. Evans, R.C. Reid, and E.M. Drake, Transient Natural Convection in a Vertical Cylinder, AIChE 14, 251-259 (1968).

4. D. Japikse, and E.R.F. Winter, Single - Phase Transport Processes in the Open Thermosyphon, Int .J. Heat Mass Transfer, 14, 427-441 (1971).

5. S. Ostrach, Natural Convection in Enclosures, ASME, Heat Transfer, 110, 1175-1190, (1988).

6. Y. Weiss, Y. Barnea, and I. Shai, Induced Mixed Convection in a Hot Gas Duct, 25th Israel Conference on Mechanical Engineering, Haifa Israel, pp. 527-529, 1994.

7. Y. Weiss., M. Szanto., I. Shai., and G. Ben-Dor., Characteristics of the Entry Flow Field in an Open Thermosyphon, The 4th Int. Conf. "Heat Transfer 96", Udine, Italy, July, pp. 83-93, 1996.

8. Y. Weiss, C. Lahav, M. Szanto and I. Shai, Heat Transfer Characteristics of Induced Mixed Convection (IMC), 26th Israel Conf. on Mechanical Engineering, Haifa Israel, pp. 300-302, 1994.

9. A. Mertol, and R. Greif, A Review of Natural Circulation Loops, in: Natural Convection Fundamentals and Applications, edited by C. Kakac., W. Aung., and R. Viskanta., Hemisphere Publishing Corporation, Washington, D.C. 1985.

10. Y. Weiss., Y. Aharon, and I. Shai, Natural Convection on a Vertical Flat Plate at General Boundary Condition, 10th Int. Heat Transfer Conf., pp. 16-NC-32, 1994.

11. J. Aharon, C. Lahav, H. Kalman, and I. Shai., An Experimental Investigation of Laminar Free Convection from a Vertical Flat Plate at General Boundary Condition, 26th Israel Conf. on Mechanical Engineering, Haifa, Israel, 1996.

12. J.R. Bodoia, and J.F. Osterle, The Development of Free Convection Between Heated Vertical Plates, Trans. ASME J. Heat Transfer, 10, 40-44 (1962).

13. A. Bar-Cohen, and W.M. Rohsemow, Thermally Optimum Spacing of Vertical, Natural Convection Cooled, Parallel Plates, Trans. ASME, J. Heat Transfer, 106, 116-123 (1984).

14. T. Burch, T. Rhodes, and S. Acharya, Laminar Natural Convection between Finitely Conducting Vertical Plates, Int. J. Heat Mass Transfer, 28, No. 6, 1173-1186, (1985).

15. B.W. Webb, and D.P. Hill, High Rayleigh Number Laminar Natural Convection in an Asymmetrically Heated Vertical Channel, Transfer, 111, 649-656 (1989).

16. L.P. Davis, and J.J. Perona, Development of Free Convection Flow of a Gas in a Heated Vertical Open Tube, Int. J. Heat Mass Transfer, 14, 889-903 (1971).

17. R. Clarksean, Experimental Analysis of Natural Convection within a Thermosyphon, Proc. Experimental Heat Transfer, Fluid Mechanics and Thermodynamics, Honolulu, Hawaii, USA, pp. 17, (1993).

18. Y. Barnea, Y. Weiss, M. Haim, and Y. Aharon, Evaluating the Dry Passive Containment Cooling of the Westinghouse AP-600 Reactor, 25th Israel Conf. on Mechanical Engineering, Haifa, Israel, pp. 518-520, 1994.

19. R. Harari, Y. Weiss, Y. Barnea, Thermohydraulic Modeling of the Dry Air PCCS Process in the Westinghouse AP-600 ALWR. The 25th Israel Conf. on Nuclear Engineering, Herzelia, Israel, pp. 7.2, 1996.

A New Generation of Gamma Cameras Based on Solid State Detectors

Y. Eisen, C. Gilath, G. Cohen, A. Shor, E. Polak, H. Cohen, Z. Baum, E. Izsac

1. Summary

The development of a new generation of gamma cameras, utilizing advanced CdTe and CdZnTe solid state detectors and offering several advantages over the present conventional cameras which employ NaI(Tl) scintillators, is described.

Nuclear Medicine is a medical imaging modality which demonstrates the organ function. It is based on administering radioisotope-labelled compounds (radio-pharmaceuticals) to the patient and then mapping distributionin space (and occasionally also in time) with gamma cameras.

The technology of present gamma cameras is based on a scheme developed by Anger some 30 years ago. The main components of a conventional gamma camera are illustrated in Figure 1. The radiation emanating from the patient is transmitted through a collimator and detected by a large NaI(Tl) scintillation crystal, which converts the incident radiation into light scintillations which are detected by a two-dimensional array of photomultipliers tubes (PMTs). The location of a scintillation in the crystal is determined by the relative signals in the adjacent PMTs. Thus an image of the radiation is obtained.
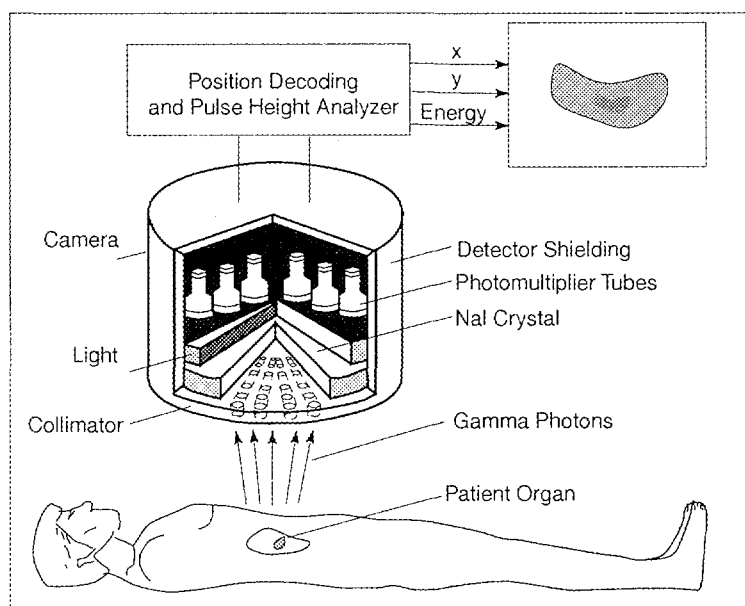
Fig. 1: Main components of a conventional gamma camera

Over the past three decades there has been a steady improvement in the original Anger camera. Image resolution and uniformity have increased and the advent of digital electronics has enabled better image correction and manipulation. However, the technology has reached a level of maturity where any real improvement can be achieved only from a radical change, as done with solid state detectors.

Scintillation type (Anger) cameras have some inherent shortcomings:

• The energy of the incident gamma radiation photon absorbed in the scintillator is transformed to light with relatively low efficiency. This implies a relatively poor energy resolution, which prevents efficient scatter rejection and thus causes deterioration in the contrast resolution. Typical energy resolution in NaI(Tl) scintillators, at the most commonly used energy in nuclear medicine, 140 Kev, is approximately 10% FWHM (full width at half maximum). It has taken present technology 30 years to get from 12% to 10%.

- Current intrinsic spatial resolution is limited by the scintillator thickness, the incident photon energy and the size and packaging ratio of the PMTs.

- Anger cameras present some image distortions (pincushion and barrel) inherent to the use of PMTs.

- At high count rates (above 100,000 counts/sec) Anger cameras suffer from pile-up distortions.

  The need for shielding both the scintillating crystal and the PMTs, which occupy a relatively large volume, results in a large, heavy and cumbersome gamma camera head. Mobile Anger gamma cameras are heavy and not practical; portable cameras are not feasible. Positioning of the camera head becomes difficult or even impossible under certain circumstances. Also tomographic gamma cameras (SPECT-single photon emission computed tomography) in which the head rotates around the patient, demand large and heavy gantries.

2. THE NEW GAMMA CAMERA TECHNOLOGY AND ACHIEVEMENTS

When X-rays or gamma photons impinge on room temperature spectroscopy grade detectors, electron - hole pairs are generated. These result in an electrical pulse carrying information on the energy of the incoming radiation. Thus, the conversion from radiation into an electrical pulse takes place in the detector itself. Solid state detectors perform the combined function of the scintillator and the PMTs in an Anger camera. CdTe and CdZnTe are more advanced solid state detectors that can be used in the new generation gamma cameras.

The use of solid state detectors in gamma cameras offers several advantages over currently used Anger scintillation cameras:

- Better (5% or even less) energy resolution, with resulting superior scatter rejection and better contrast resolution in the resulting image. The lower the energy resolution, the better the image quality. This attribute becomes

important with large-size patients (who already provide increased radiation absorption between the organ of interest and the camera head) and many newer nuclear medicine procedures in which the target organ to background ratio is relatively low (e.g. scintimammography and the use of labelled monoclonal antibodies or peptides for imaging of malignant lesions). Improved contrast resolution leads to improved detectability of lesions.

- Better intrinsic spatial resolution can be achieved. Spatial resolution is dependent neither on the detector thickness nor on the incident photon energy, but only on the detector element area size. This attribute manifests itself in improved image quality and better spatial resolution and therefore contributes to improved detectability.

- The use of solid state detectors removes the need for the photon interaction position decoding (as necessary in Anger cameras). The position of the interaction is defined by the detector element in which the interaction takes place. Perfectly linear and homogeneous images are obtained, without any geometric distortions (barrel and cushion).

- Solid state detectors are-count-rate tolerant and for all practical purposes no pile-up distortions are observed.

- Much lighter camera heads become feasible. The heads are very thin compared with conventional ones, since no long PMTs are used.

- Mobile and portable gamma camera systems become practicable. They enable bringing the imaging to the patient rather than transporting a critically ill patient to the camera and taking unacceptable risks. Furthermore, patients can be diagnosed at any location in the hospital, office or even their home.

- Planar and tomographic (SPECT) cameras can be built with much simpler mechanics than conventional cameras. This leads to cost reduction and a decrease in the system footprint, a practical aspect that should not be ignored.

- The area of the camera head face is nearly equal to the useful field of view. This enables imaging of locations

on the body at much closer proximity than with an Anger camera head, a feature very important in breast, thyroid, parathyroid and other imaging protocols.

- The thermal stabilization of the camera head is very rapid. (Present Anger cameras are kept constantly under power and heavy battery backups are used when attempting mobile configurations).

- Current technology still relies on vacuum tubes. Replacing the PMTs with solid state devices improves system stability and reliability.

Soreq NRC has amassed 15 years of experience with room temperature solid state CdTe and lately also with CdZnTe detectors. Various detectors were designed and characterized, and applications were developed for security inspections of cargo and passenger luggage. One of these applications culminates in the Aisys 370 automatic luggage inspection and bomb detection system (protected by several patents), the manufacture of which was licensed to Magal Security Systems Ltd. From the early 1990s various medical applications of these detectors were considered and explored. It was decided to focus on the development of gamma cameras. The practical and business values of this application were recognized by the Chief Scientist of the Israel Ministry of Trade and Industry, who provided partial financial support for this development effort.

At a later stage, the United States Israel - Science and Technology Commission undertook to fund the development of a new generation of gamma cameras based on solid state detectors. A collaboration among Isorad Ltd. (the commercial arm of Soreq NRC), General Electric Medical Systems and eV Products, Inc. (a developer and manufacturer of solid state detectors) was set up. The

objective of this project is to develop, engineer, manufacture and market the new gamma cameras in a cost effective way. CdZnTe detectors were chosen for this development.

Two camera prototypes were developed. One of them, in a mobile planar configuration with a head having a field of view of 16 cm x 16 cm, is shown in Figure 2. Figure 3 illustrates the prototype camera ready for use in a hospital emergency room. Soreq NRC's efforts were concentrated on the development of the new head, which is central to the performance of the camera and represents the most innovative part of the system. In addition, emphasis was placed on the development of the necessary acquisition, processing and display software. Soreq's developments are protected by several patents.

Fig. 2: The prototype for a new generation gamma camera based on solid state detectors.
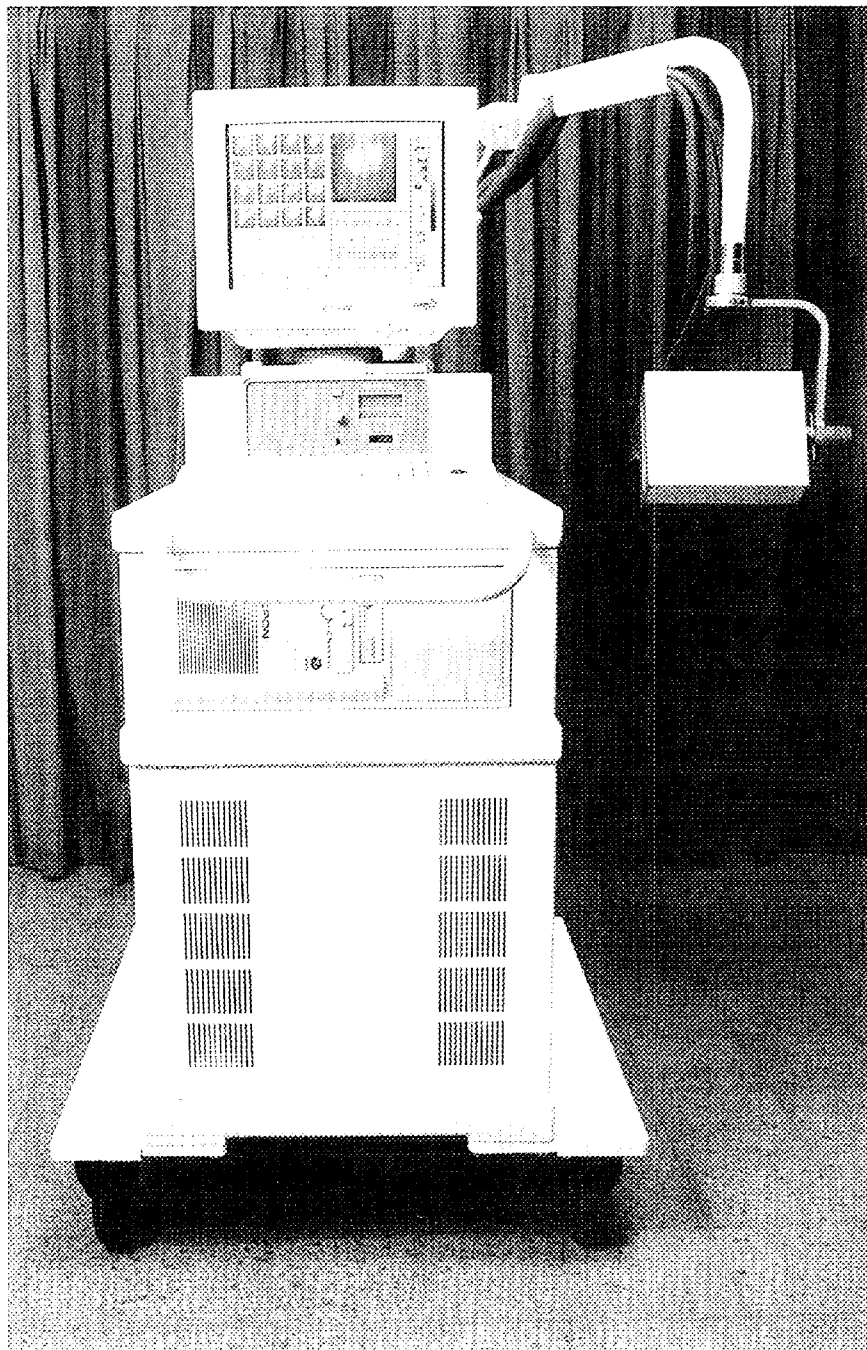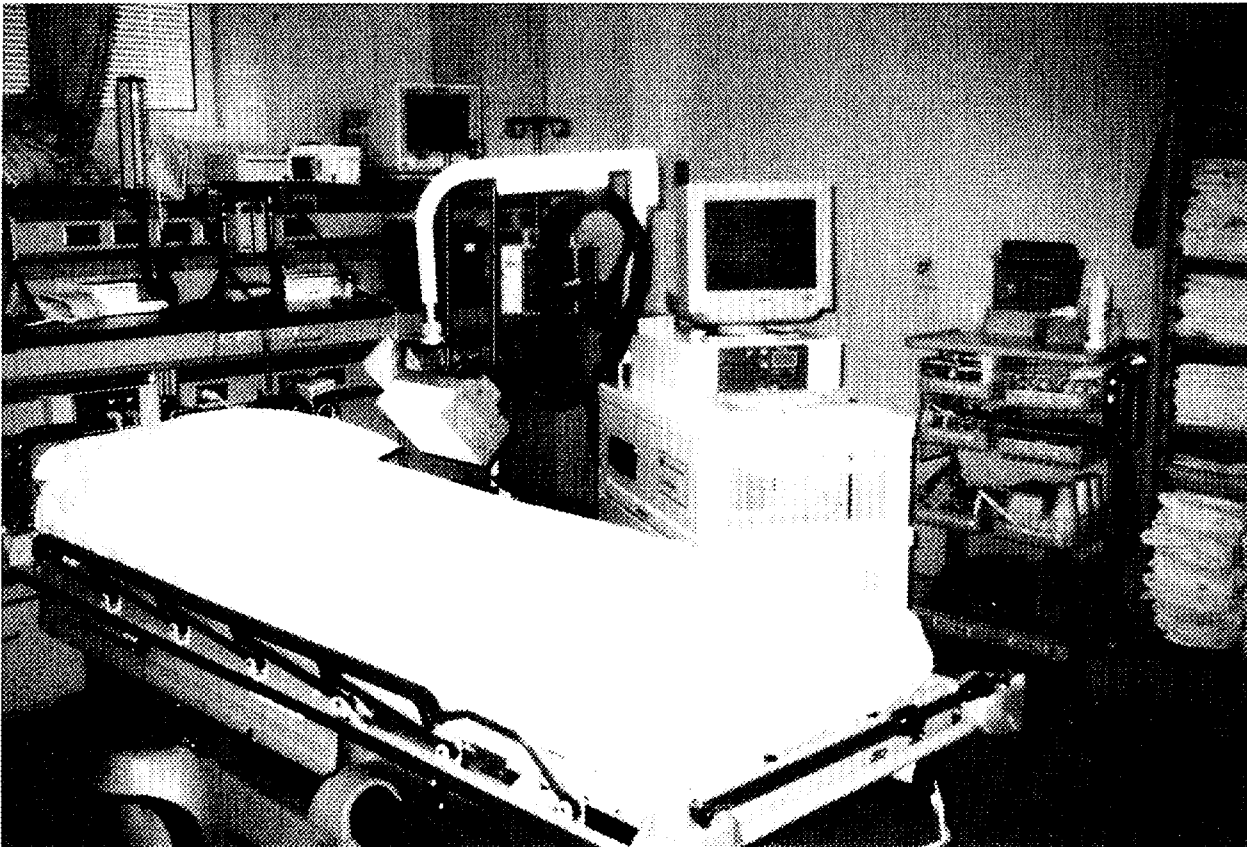
Fig. 3: The prototype camera in the emergency room of a major US hospital.

The prototype was evaluated in various clinical environments, first in Israel and then in the USA and Canada. Some typical images obtained with this prototype are shown here. Common nuclear cardiology procedures, such as MUGA (multiple gated angiography) which implies ECG gating (see Fig. 4) and myocardial perfusion imaging (see Fig. 5), were performed. Various other nuclear medicine procedures, such as thyroid (see Fig. 6), parathyroid, breast, and kidney imaging, etc., were also performed.

The diagnostic capability of the prototype camera was found to be similar or superior to that of conventional cameras. The mobility of the camera and the ease of positioning its head on the patient were greatly appreciated by both physicians and technical personnel. The potential of solid state-detector-sbased gamma cameras was proven.

Work on the United States-Israel Science and Technology Commission project continues towards the achievement of its technological and commercial objectives.

Fig. 4: Results of a MUGA (multiple gated angiography) procedure performed with the prototype camera and compared with a conventional camera.
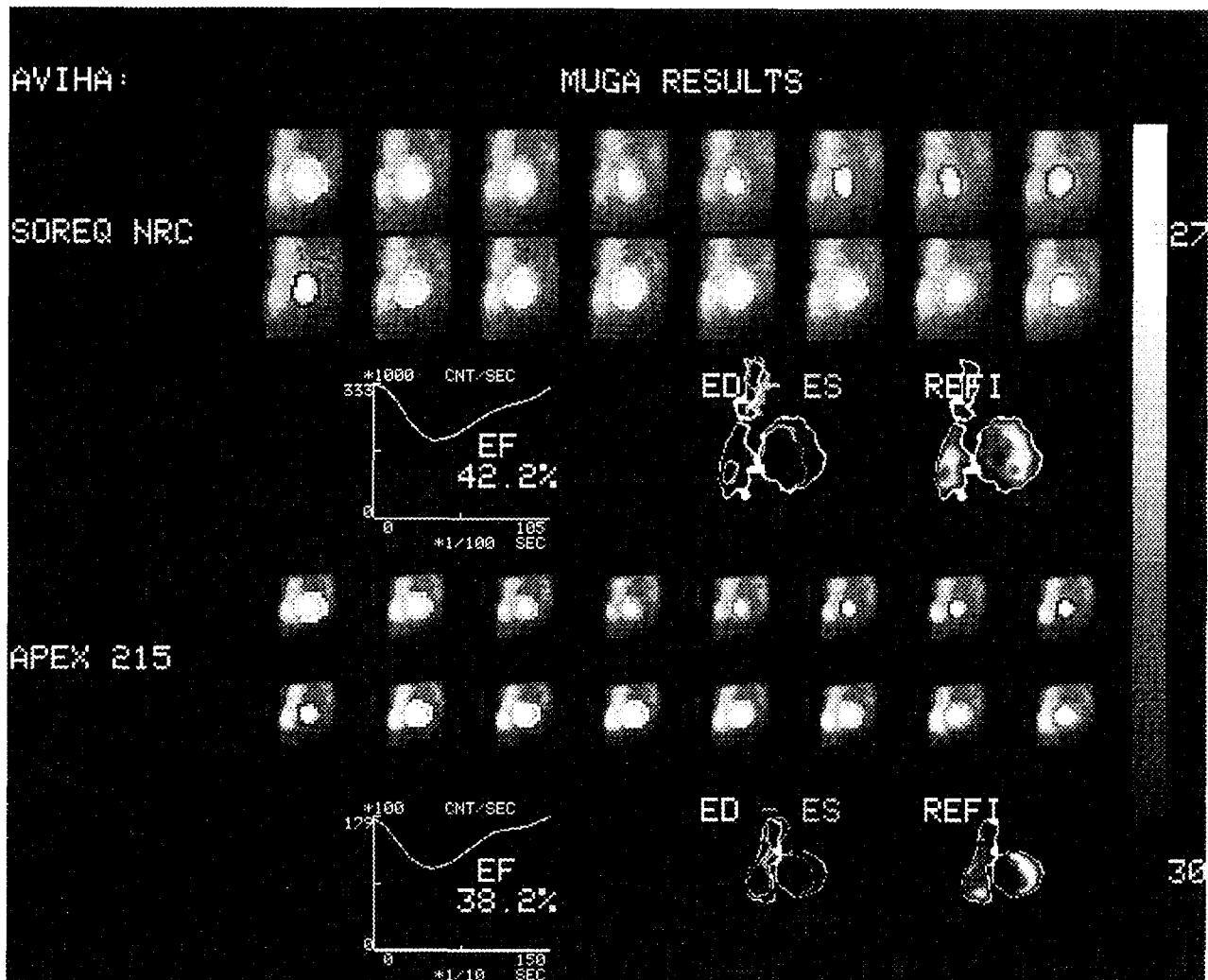
Fig. 5: Results of a myocardial perfusion procedure performed with the prototype camera.
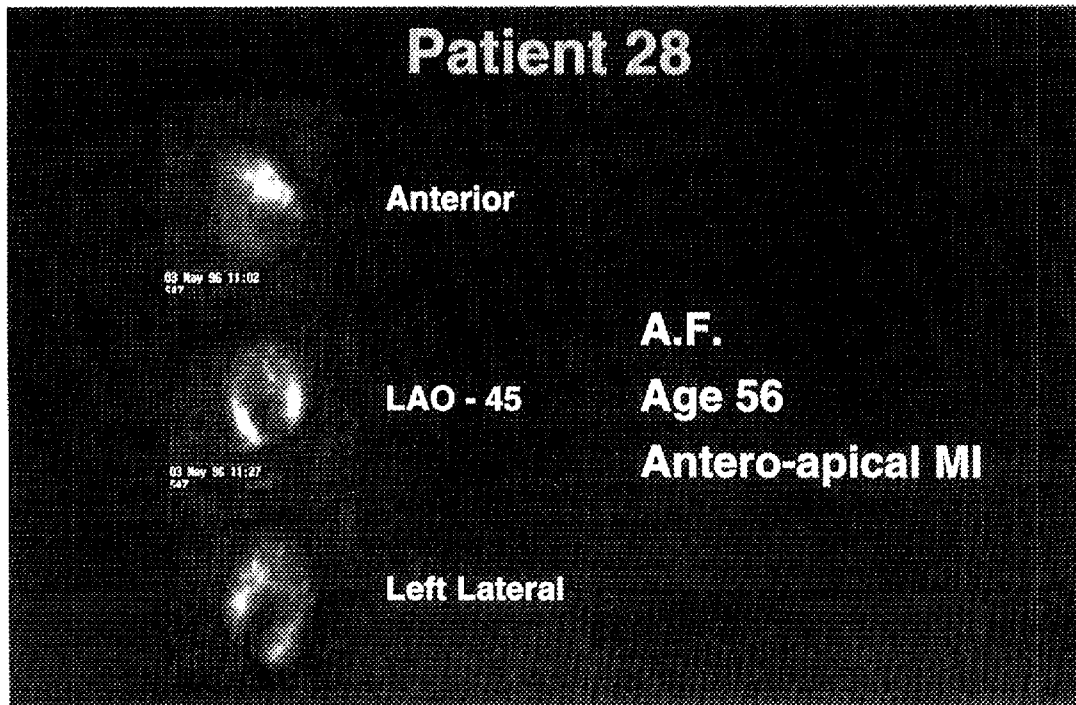

Fig. 6: Results of thyroid imaging performed with the prototype camera.